


DISTURBANCES OF IONOSPHERIC RADIO CHANNEL DURING MAGNETIC STORMS IN NOVEMBER–DECEMBER 2023

S.N. Ponomarchuk 

Institute of Solar-Terrestrial Physics SB RAS,
Irkutsk, Russia, spon@iszf.irk.ru

N.A. Zolotukhina 

Institute of Solar-Terrestrial Physics SB RAS,
Irkutsk, Russia, zolot@iszf.irk.ru

Abstract. This paper presents the results of analysis of oblique ionospheric sounding data obtained with continuous chirp signal on the subauroral paths Magadan—Irkutsk and Norilsk—Irkutsk. It specifies the interplanetary sources of magnetic storms in November–December 2023. It has been established that signals propagating outside the great-circle arc and additional diffuse reflections can be found in oblique sounding ionograms in intense magnetospheric convection field. Their appearance can be related to refraction of radio waves on the polar wall of the main ionospheric trough and scattering by small-scale inhomogeneities. Connec-

tion has been revealed between variations in the maximum observed frequencies of HF radio wave propagation modes with the spatial position of the main ionospheric trough and the equatorial boundary of diffuse electron precipitation zone.

Keywords: radio wave propagation, radio channel, magnetosphere, high-latitude ionosphere, oblique ionospheric sounding, main ionospheric trough, diffuse electron precipitation.

INTRODUCTION

Properties of the ionospheric radio channel depend on many factors, the main of which are the processes of energy supply from the heliosphere to the outer geospheres (magnetosphere, ionosphere, and thermosphere). Enhancement of incoming energy flux causes magnetospheric disturbances such as geomagnetic storms, which are accompanied by ionospheric disturbances of various types (ionospheric storms) that alter propagation conditions of HF radio waves. Study of such disturbances is important both for understanding geophysical phenomena in the magnetosphere—ionosphere system and for solving practical problems of ionospheric propagation of radio waves [Blagoveshchensky, Zherebtsov, 1987; Hunsucker, Hargreaves, 2003; Blagoveshchenskii, 2013; Warrington et al., 2017].

On subauroral paths, large-scale structures characteristic of the high-latitude ionosphere such as the auroral oval and the main ionospheric trough (MIT), as well as small-scale magnetic field-aligned irregularities, have the greatest effect on radio wave propagation conditions. During geomagnetic storms, the auroral oval and MIT shift to lower latitudes [Zherebtsov et al., 1988; Blagoveshchensky, Borisova, 2000; Uryadov et al., 2004; Kurkin et al., 2006], thereby causing strong variations in maximum observed frequencies (MOF) of propagation modes in oblique sounding (OS) ionograms [Blagoveshchensky et al., 2008; Polekh et al., 2016], deviation of signal propagation paths from the great circle arc [Hunsucker, Bates, 1969; Rogers et al., 1997; Zaalov et al., 2003], occurrence of abnormal signals with delays exceeding the delays of the main modes, and diffuse signals [Rogers et al., 2003; Kurkin et al., 2004; Uryadov et al., 2004; Uryadov et al., 2005; Blagoveshchenskii, 2016].

The purpose of this work is to examine the manifestation of heliosphere-geosphere coupling in OS data from the subauroral HF radio paths Magadan—Irkutsk and Norilsk—Irkutsk during geomagnetic storms in November–December 2023.

1. GEOMAGNETIC STORMS AND THEIR HELIOSPHERIC (INTERPLANETARY) SOURCES

Geomagnetic storms in November–December 2023 have been analyzed using K_p [<https://kp.gfz-potsdam.de/en/data>], Dst [https://wdc.kugi.kyoto-u.ac.jp/dst_realttime/index.html], solar wind (SW) and interplanetary magnetic field (IMF) parameters ahead of near-Earth shock front [https://cdaweb.gsfc.nasa.gov/cdaweb/istp_public/]. The $SYM-H$ indices were also used [https://cdaweb.gsfc.nasa.gov/cdaweb/istp_public/] which are related to the symmetric ring current; SME [<http://supermag.jhuapl.edu/indices/>] — an analog of AE characterizing the activity of an auroral electrojet [Bergin et al., 2020]; Dst^* — corrected for SW pressure (P_{sw}) Dst , from which the contribution of the Chapman—Ferraro current flowing at the magnetopause was subtracted [Burton et al., 1975]:

$$Dst^* = Dst - 16P_{sw}^{1/2} + 20.$$

The heliospheric sources were determined from the information posted at [<ftp://ftp.swpc.noaa.gov/pub/warehouse/>] and [http://www.solen.info/solar/old_reports/], with additional data on sources of storms [http://www.solen.info/solar/coronal_holes.html], [https://cdaw.gsfc.nasa.gov/CME_list/].

The Akasofu parameter [Akasofu, 1981] was employed to estimate the SW electromagnetic energy flux incident on the front of the magnetopause [Dremukhina et al., 2018].

There are the following designations in the text: V_{sw} — SW velocity; N_{sw} — SW ion concentration; P_{sw} — SW dynamic pressure; IMF B_t — IMF modulus; IMF B_z — vertical component of IMF in the solar-magnetospheric coordinate system GSM; ε — Akasofu parameter; SI_{sym} — sudden increase in *SYM-H*; CME — coronal mass ejection; ICME — interplanetary coronal mass ejection; CH — coronal hole; CHHSS — coronal hole high speed stream.

When describing geomagnetic storms, we apply the concept of multi-step geomagnetic storm whose need is justified, for example, in [Kamide et al., 1998; Richardson, Zhang, 2008]. This concept refers to geomagnetic storms whose main phase consists of several intervals of amplification of the ring current (decreases in *Dst*), separated by intervals of its partial attenuation (*Dst* increase).

1.1. Brief overview on interplanetary and geomagnetic conditions

From K_p and *Dst* (Figure 1) in November and December 2023, we can identify eight long-lasting geomagnetic disturbances with minimum $Dst < -30$ nT. According to [Gonzalez et al., 1994], these disturbances are geomagnetic storms. The storms, numbered in chronological order, are listed in Table. According to the classification proposed in [Loewe, Prolss, 1997], storm 2 is weak, storms 3, 4, 6–8 are moderate, and storms 1 and 5 are severe. In Table, the rows containing information on the weak storm, moderate and severe storms are colored in gray, blue, and terracotta respectively. There are noticeable differences between minimum *Dst* and Dst^* (Figure 1, *b*, *e*) associated with high P_{sw} during storms and hence with amplified Chapman—Ferraro currents. The difference between Dst^* and *Dst*, equal to -52 nT, is maximum for storm 5. The highest peak values of $\varepsilon \approx 7000$ GW correspond to severe storms 1 and 5. In other storms, the maximum values of $\varepsilon \leq 1 \div 1.5$ GW.

Comparing the variations in K_p , *Dst*, and V_{sw} (Figure 1), it can be observed that all magnetic storms are related to high-speed SW streams. Brief information on the interplanetary structures that formed them is given in the last column of Table.

The relationship between tabulated CHHSS and their associated storms is confirmed by the data from [http://www.solen.info/solar/coronal_holes.html]. The number of ICMEs indicated in Table for storms 2, 3, and 5–8 corresponds to the list of geoeffective CME types "halo" or "partial halo", presented at [https://cdaw.gsfc.nasa.gov/CME_list/]. According to the CME list, 9 and 2 ICMEs could contribute to the formation of sources of storms 1 and 4 respectively, rather than 3 and 1 ICMEs.

1.2. Storm 1

The severe storm on November 4–10, 2023 consisted of an initial phase, a three-step main phase, and a long five-day recovery phase, as inferred from *Dst* and *SYM-H* variations (Figure 2, *a*). Thirty and fifty minutes before the onset of the second and third steps of the main phase, there were sharp increases in *SYM-H* by 29

and 37 nT respectively. By the time of their occurrence, they correspond to the arrival of interplanetary shocks at Earth's magnetosphere, observed by SOHO on November 5 at 08:13 and 11:55 UT [http://www.solen.info/solar/old_reports/].

Such sharp increases in *SYM-H* may be manifestations of sudden impulses (SI [Joselyn, Tsurutani, 1990]) caused by jumps in P_{sw} . The authors of the cited work believe that an event can be identified with SI only if it is recorded simultaneously (within a few minutes) by the worldwide network of observatories located near the geomagnetic latitude of 20° . Since only *SYM-H* is used in this work to identify such events; hereinafter, we designate them not as SI, but as $SI_{sym} N.I.$, where N is the storm number; I is the event number in this storm in chronological order.

The initial phase and each of the three *Dst* decreases (see Figure 2), identified with steps 1–3 of the storm main phase, coincide in time with the passage of interplanetary structures with large N_{sw} ($40\text{--}50 \text{ cm}^{-3}$), B_t ($15\text{--}35$ nT), and southward vertical IMF component ($B_z \sim -(11\text{--}23)$ nT) through Earth's orbit. Black arrows indicate two sudden increases in *SYM-H*: $SI_{sym}1.1$ and $SI_{sym}1.2$. The time intervals corresponding to the initial phase and three steps of the main phase are marked with green and three gray rectangles. Similar structures with large N_{sw} and B_t are formed in front of CMEs with velocities exceeding the velocity of SW located in front of them. They are commonly called CME sheaths [Kilpua et al., 2017].

In isolated ICMEs, the transition from sheath to CME per se is accompanied by decreases in N_{sw} , plasma temperature, and plasma beta [Davies et al., 2020]. In the complex interplanetary disturbance (Figure 2, *b–d*), presumably formed by several ICMEs, decreases in N_{sw} behind three sheaths (colored rectangles) were not followed by decreases in temperature and plasma beta (omitted in Figure 2). We believe that this is due to a more complex structure of the interplanetary source of storm 1 than it follows from [<ftp://ftp.swpc.noaa.gov/pub/warehouse>] and [http://www.solen.info/solar/old_reports/]. According to [https://cdaw.gsfc.nasa.gov/CME_list/], during the days preceding the storm (October 31, November 2, November 3, 2023), not 1, but 3, 2, and 4 partial halo CMEs were observed respectively, which formed the interplanetary structure that drove the initial and main phases of storm 1. Analysis of the formation of this structure from nine ICMEs during their motion from the Sun to Earth's orbit is beyond the scope of this work.

Note that for each sheath there are peaks of ε (see Figure 1) and *SME* (bottom panel in Figure 2). During the early recovery phase of the storm (November 6), the magnetosphere-ionosphere system was under the weakening influence of the last ICME and CHHSS from coronal hole CH1183; during the late one (November 7–10), under the influence of the same CHHSS that did not cause a significant increase in auroral activity.

1.3. Storm 2

Figure 3 shows that the November 12–14, 2023 disturbances, including weak storm 2, began on November 12 at 06:12–06:15 UT with a sudden impulse ($SI_{sym}2.1$, indicated by an arrow) 40 min after detecting a weak shock in

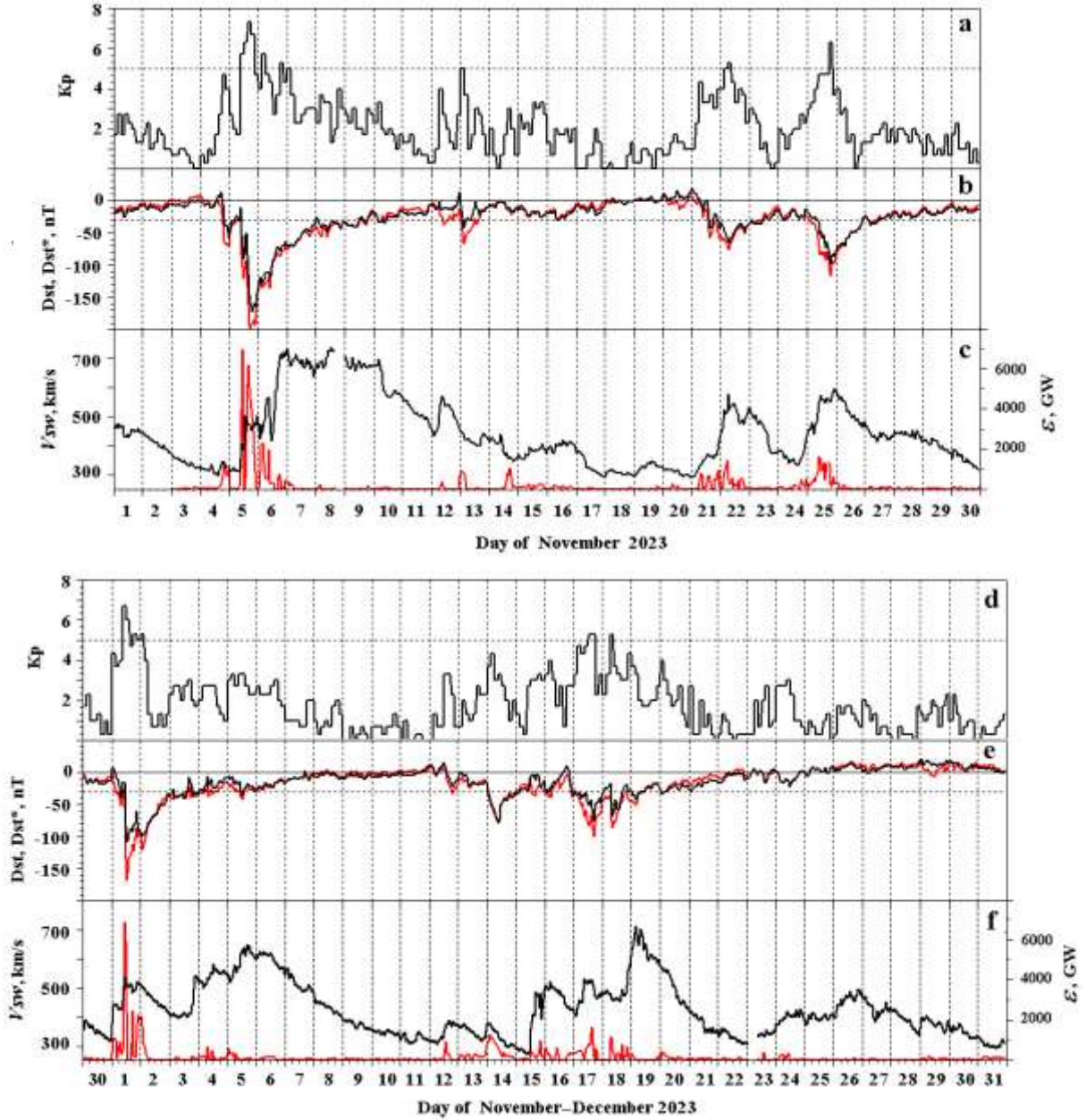


Figure 1. Variations in K_p (a), Dst , and Dst^* (black and red lines respectively, b), V_{sw} (black line, c), ϵ (red line) in November (a–c) and December (d–f) 2023. Horizontal dotted lines on panels a, b, d, e mark $K_p=5$ and $Dst=-30$ nT, used to identify magnetic storms

Geomagnetic storms in November–December 2023, their associated extreme K_p , Dst indices, and interplanetary sources

Storm number	Duration	Maximum K_p	Minimum Dst	Possible interplanetary sources	
				Main phase	Recovery phase
1	Nov. 04–10, 2023	7.3	–172	3 ICME of Oct. 31, 2023, Nov. 02, 2023, Nov. 03, 2023	ICME of Nov. 03, 2023; CHSS from CH1183
2	Nov. 12–14, 2023	5.0	–42	ICME of Nov. 09, 2023	CHSS from CH1184
3	Nov. 21–23, 2023	5.3	–65	CHSS from CH1187	
4	Nov. 25–26, 2023	6.3	–99	ICME of Nov. 22, 2023	CHSS from CH1189
5	Dec. 01–07, 2023	6.7	–108	2 ICME of Nov. 27, 2023, Nov. 28, 2023	ICME of Nov. 28, 2023, Dec. 01, 2023; CHSS from CH1190
6	Dec. 13–15, 2023	4.3	–78	CH HSS from CH1192	
7	Dec. 16–18, 2023	5.3	–76	3 ICME of Dec. 13–15, 2023	
8	Dec. 18–21, 2023	5.3	–68	ICME of Dec. 15, 2023 (?); CHSS from CH1193	CHSS from CH1193

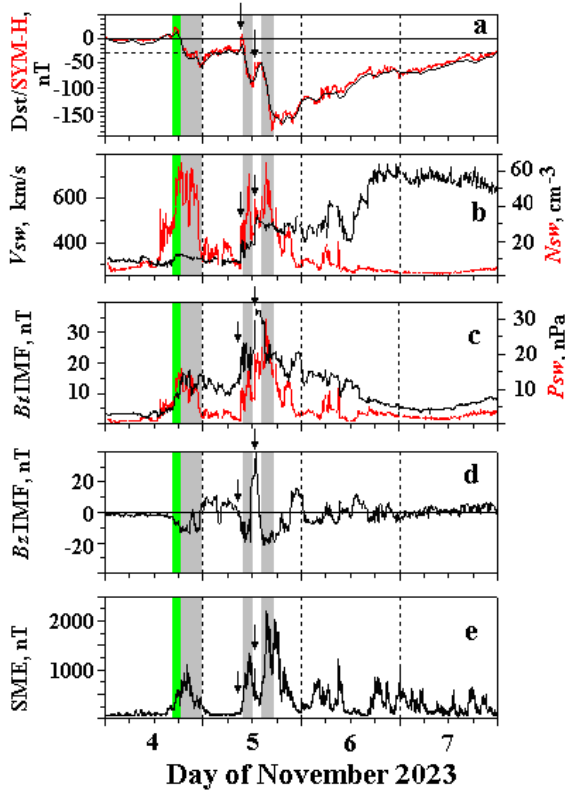


Figure 2. Variations during severe magnetic storm 1: *a* — $Dst/SYM-H$ (black/red line); *b* — V_{sw}/N_{sw} (black/red line); *c* — B_z/P_{sw} (black/red line); *d* — B_z ; *e* — SME . Green rectangles represent the initial phase of the storm; gray ones, three steps of its main phase

interplanetary space [<ftp://ftp.swpc.noaa.gov/pub/warehouse/>]). During $SI_{sym2.1}$, $SYM-H$ increased from -9 to 11 nT. $SI_{sym2.1}$ was followed by an increase in auroral activity, comparable in maximum of $SME \sim 750$ nT with that occurring at the first step of the main phase of storm 1.

From $SI_{sym2.1}$ to ~ 12 UT on November 13, geospheric disturbances were driven by November 9 ICME, designated as halo CME during its formation [https://cdaw.gsfc.nasa.gov/CME_list/]. Then, until ~ 9 UT on November 17, the main source of disturbances was CHSS from CH1184.

The SW regions responsible for the development of the initial phases of storms 1 and 2 are similar in large N_{sw} , P_{sw} , and B_z , but they differ in direction of B_z . In the former case, $B_z < 0$; in the latter, mainly $B_z > 0$. Responses to their impact in SME also differ. During the initial phase of storm 1, SME increased to ~ 500 nT; during the initial phase of storm 2, it remained unchanged, ~ 200 nT. Just as during three steps of the main phase of storm 1, to the main phase of storm 2 corresponds in time the passage of the SW region with high N_{sw} , P_{sw} , B_z , and southward B_z through Earth's orbit, as well as an increase in auroral activity (see Figures 2, 3).

1.4. Storms 3, 4

A series of geomagnetic disturbances, including moderate storms 3 and 4, began after the magnetically quiet days of November 16–20 [http://www.solen.info/solar/old_reports] and [<ftp://ftp.swpc.noaa.gov/pub/warehouse/>].

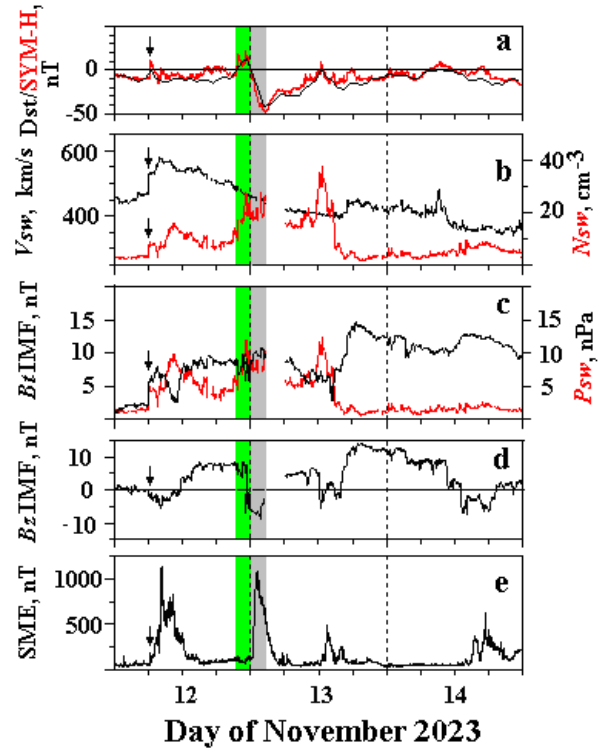


Figure 3. The same as in Figure 2 for weak geomagnetic storm 2

These two storms have interplanetary sources of different types. Storm 3 was caused by CHSS from CH1187; storm 4, by a combined effect of one (possibly two) ICME and CHSS from CH1189.

Storm 3 started on November 21 after 13:00 UT and ended on November 23 at $\sim 24:00$ UT. The interplanetary source of this storm features B_z variations with periods $T \sim 6-8$ hrs and ~ 15 nT amplitude (Figure 4, *d*). The first decrease in B_z to -8 nT, observed 6 hrs before the onset of storm 3, occurred at relatively low $N_{sw} \sim 10$ cm^{-3} and $P_{sw} \sim 1.5$ nPa. It caused a slight decrease in Dst to ~ -8 nT and a noticeable increase in SME to ~ 600 nT. Steps 1–3 of the storm main phase with minimum $Dst = -42$, -42 , and -63 nT and increases in SME to 1000, 700, and 1300 nT respectively are linked to SW regions with relatively high N_{sw} , P_{sw} , B_z , and southward IMF z component ($B_z < 0$). Nonetheless, if N_{sw} and P_{sw} remain high throughout steps 1 and 2 (> 15 cm^{-3} and > 4 nPa respectively), then, as step 3 develops, N_{sw} and P_{sw} decrease from 16 to 5 cm^{-3} and from 4.6 to 3 nPa respectively.

The main phase of moderate magnetic storm 4 developed on November 25 at $\sim 09-19$ UT under the action of November 22 ICME (possibly two ICMEs associated with two partial halo CMEs [https://cdaw.gsfc.nasa.gov/CME_list/]). It consisted of two steps. Attenuation of the ring current (Dst and $SYM-H$) between the two steps was followed by a short-term weakening of B_z . During the hours preceding the storm on November 24 and 25, spacecraft detected transient disturbances, which caused a decrease in Dst to -31 , -28 nT and an increase in K_p to 2.7.

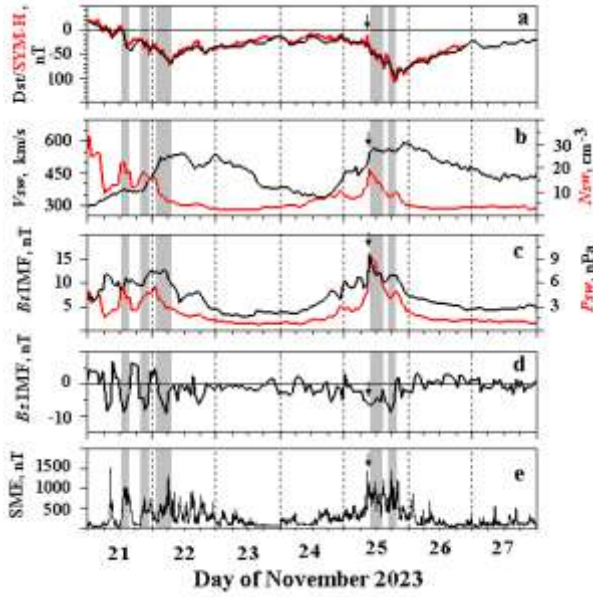


Figure 4. The same as in Figures 2, 3, for moderate geomagnetic storms 3 and 4

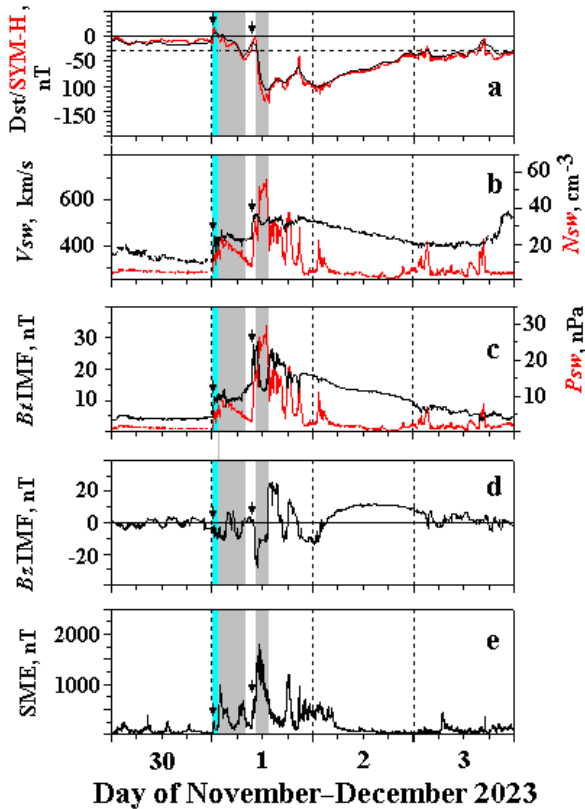


Figure 5. The same as in Figures 2, 3, for the first days of strong geomagnetic storm 5

An hour before the beginning of the main phase at 08:36–08:38 UT on November 25, there was a sharp increase in $SYM-H$ (SI_{SYM} 4.1) by 19 nT, related to the interplanetary shock recorded by SOHO on November 25 at 08:00 UT [http://www.solen.info/solar/old_reports/]. The dominant contribution to the development of the storm recovery phase, which lasted until the end of November 26, was made by CHSS from CH1189.

1.5. Storm 5

The December 1–7, 2023 severe magnetic storm consisted of a 65-min initial phase followed by a 12-hr two-step main phase and a long six-day recovery phase (Figure 5). Interplanetary sources of the storm were three ICMEs formed on November 27, 28, and December 1, and CHSS from CH1190 [http://www.solen.info/solar/old_reports/]. The November 27 ICME gave rise to $SI_{SYM}5.1$, the initial phase, and the first step of the main phase of the storm on December 1 at 00:20–00:23 UT; the November 28 ICME became an interplanetary source of $SI_{SYM}5.2$, observed on December 2 at 09:25–09:27 UT, and the second step of the main phase of storm 5, which began an hour after it. Interplanetary shocks corresponding to $SI_{SYM}5.1$ and $SI_{SYM}5.2$ were recorded by SOHO on November 30 at 23:39 UT and on December 1 at 08:50 UT.

The early recovery phase of the storm was associated with the weakening effect of the second ICME. It began on December 1 at ~12:30 UT and ended at ~22:00 UT that day with another decrease in Dst , which run to -100 nT by 01:30 UT on December 2, which is comparable to $Dst=-108$ nT that is minimum for storm 5 (see Table). In this case, the decrease in Dst was caused by the combined effect of amplification of the ring current and attenuation of Chapman–Ferraro currents flowing at the magnetopause, which was caused by a sharp decrease in P_{sw} [Zhao et al., 2011]. This is confirmed by the Dst^* variation in December 2023 (see Figure 1). At storm maximum, minimum $Dst^*=-160$ nT, and it decreased to 114 nT by the end of December 1 – beginning of December 2.

The late recovery phase of storm 5 developed due to December 1 ICME and CHSS from CH1190. It ended on December 7 at ~24 UT.

1.6. Storms 6–8

The sites listed at the beginning of Section 1 present only some of possible interplanetary sources of magnetic disturbances shown in Figure 6, including moderate storms 6–8. For the weak disturbances observed on December 12, this is a flow from a small coronal hole of negative polarity or a transient process from CME [http://www.solen.info/solar/old_reports/]. The source of moderate storm 6, which began at the end of December 13 and ended with $SI_{SYM}6.1$ on December 15 at noon, was CHSS from CH1192 [http://www.solen.info/solar/old_reports/] and [http://www.solen.info/solar/coronal_holes.html]. A shock corresponding to $SI_{SYM}6.1$ was detected by SOHO on December 15 at 11:05 UT.

During moderate storm 7 (December 16–18), a complex interplanetary structure, formed by several ICMEs of December 12–15 including ICME recorded as halo CME on December 14, passed through Earth's orbit [https://cdaw.gsfc.nasa.gov/CME_list/]. The most likely source of the geomagnetic disturbances on December 18 to 18 UT was ICME; and from 18 UT on December 18 to the end of December 21, CHSS from CH1193.

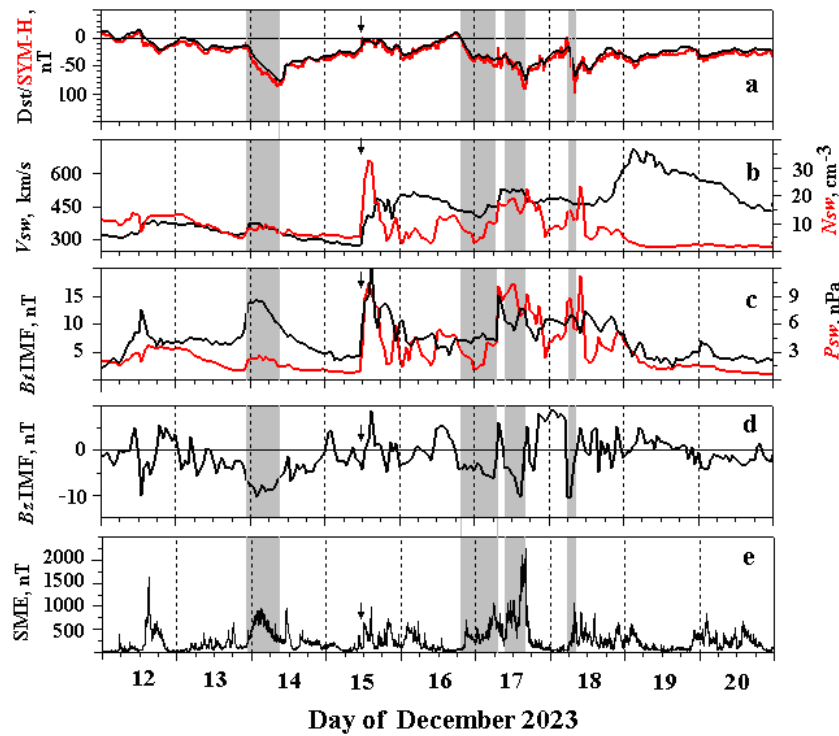


Figure 6. The same as in Figure 4 for moderate geomagnetic storms 6–8

2. ANALYSIS OF EXPERIMENTAL OS DATA

The effect of the magnetic storm on radio wave propagation conditions in the ionospheric radio channel has been studied by analyzing experimental data on radio paths located in northeastern Russia: Magadan—Irkutsk ($l=3034$ km, longitude of the midpoint $\lambda=124.21^\circ$ E, invariant $\Phi=53.31^\circ$) and Norilsk—Irkutsk ($l=2030$ km, $\lambda=97.54^\circ$ E, $\Phi=56.92^\circ$). Transmitting stations are located near Magadan (60° N, 150.7° E) and Norilsk (69.4° N, 88.4° E); the receiving station Irkutsk, in the village of Tory, Buryatia (51.8° N, 103° E). This network of radio paths operates on the basis of a spatially distributed multifunctional chirp ionosonde, developed at ISTP SB RAS [Podlesnyi et al., 2013; Kurkin et al., 2024]. Geometry of the paths is demonstrated in

Figure 7. Note that the meridional path Norilsk—Irkutsk is a path of quasi-longitudinal radio wave propagation relative to the geomagnetic field, and Magadan—Irkutsk is a path of quasi-transverse radio wave propagation. All the stations are equipped with timing and synchronizing devices. Sounding along the paths was performed at an interval of 5 min.

To process a large body of OS ionograms (~ 34000), we have automatically processed and interpreted the ionograms [Grozov et al., 2012; Ponomarchuk, Grozov, 2024; Ponomarchuk et al., 2024] and have used the results to plot time dependences of MOF of one hop propagation mode for signals reflected from the F-region (MOF_{IF}).

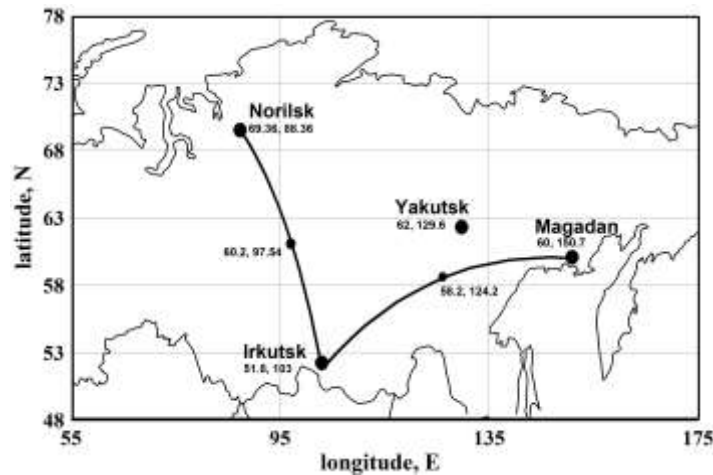


Figure 7. Geometry of OS paths in northeastern Russia

The algorithm for interpreting ionograms involves using the results of modeling the distance-frequency characteristic (DFC) of signal propagation along a given path in the long-term prediction mode, adiabatic invariants, and the results of secondary processing of experimental ionogram — points with a significant amplitude [Ponomarchuk, Grozov, 2024]. This yields the frequency dependence of the group path of the propagation mode $P^{\text{real}}(f)$, linked to the point (f_m^r, P_m^r) , where f_m^r is the maximum usable frequency (MUF) of the mode; P_m^r is the group path of the closing point of upper and lower rays [Davis, 1973]. Figure 8 exhibits an OS ionogram obtained on November 5, 2023 from the Magadan—Irkutsk path, and the results of interpretation of propagation modes. We have identified propagation modes 1F2, 2F2, and 3F2 and have plotted corresponding $P^{\text{real}}(f)$ (red dashed lines). The frequency f_m^r is related to points with significant amplitude, so hereinafter we conditionally call it propagation mode MOF. Red arrows indicate the position of the point (f_m^r, P_m^r) for each propagation mode.

During severe magnetic storms at local night time, additional diffuse signals in addition to regular propagation modes were recorded in experimental OS ionograms. Delays in such signals are generally longer than delays in regular propagation modes. Such an ionogram obtained from the Magadan—Irkutsk path on November 4, 2023 at 19:35 UT is exemplified in Figure 9. Along with standard propagation mode 1F2 there was an abnormal diffuse 1F signal in the ionogram. Its appearance might have been caused both by azimuthal refraction in transverse electron density gradients of large-scale irregularities in MIT [Zaalov et al., 2003, 2005] and by reflection from the polar wall of MIT when it approaches the region of reflection of signals on the propagation path [Kurkin et al., 2004; Uryadov et al., 2004]. Signal diffusivity can be due to both radio wave scattering by intense small-scale field-aligned irregularities [Basler et al., 1988; Uryadov et al., 2004; Uryadov et al., 2005] and refractive forward scattering by irregularities near MIT [Zaalov et al., 2005].

The method of model mask embedded in the algorithm of interpreting OS ionograms, which was constructed based on the results of calculation of OS DFC, allows us to interpret individual signals in the ionogram from points with significant amplitude. In Figure 9, the result of interpretation of $P^{\text{real}}(f)$ for an abnormal diffuse signal is indicated by the red line and designated as 1F. Standard propagation mode 1F2 was not identified because the point (f_m^r, P_m^r) is found from the maximum of the distribution of points with significant amplitude, which fall into the model mask when it moves along the ionogram. The curve $P^{\text{real}}(f)$ is seen to describe additional diffuse 1F signal well, which indicates the refractive mechanism of propagation of scattered signals in the

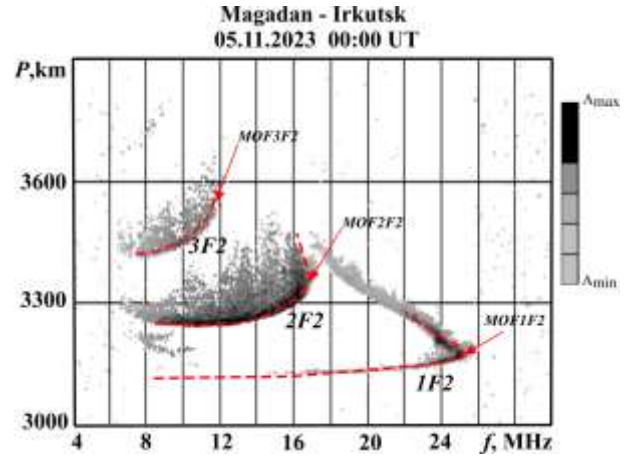


Figure 8. OS ionogram and interpretation results for November 05, 2023, 00:00 UT. The ionogram is marked with gray and black dots; $P^{\text{real}}(f)$, with red dashed lines

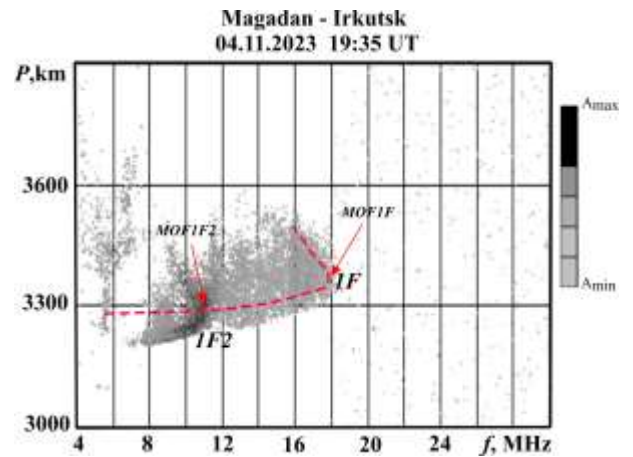


Figure 9. OS ionogram and interpretation results for November 04, 2023, 19:35 UT. Gray and black dots mark the ionogram; $P^{\text{real}}(f)$ is indicated by red dashed lines

ionosphere. The frequency f_m^r can also be taken as one hop propagation mode MOF (MOF_{1F}). The test comparison between the results of manual and automatic ionogram processing for disturbed conditions has shown that the standard deviation of the relative error in determining MOF was less than 5%. In what follows, we analyze variations in MOF_{1F} obtained by automatic processing of experimental OS ionograms without separating standard and anomalous signal propagation modes. The mode structure of the signal during ionospheric disturbances is analyzed in detail using experimental ionograms.

To interpret features of the mode structure of HF signals and MOF_{1F} variations, we employ the results of modeling of invariant latitudes of the MIT bottom [Deminov, Shubin, 2018] and the equatorial edge of the diffuse precipitation zone (DPE) of ≥ 100 eV electrons [Kamide, Winningham, 1977], as well as the magnetospheric convection field strength E_c [Burke et al., 2007]. Electrons with an energy of ~ 100 eV penetrate into the F-region of the ionosphere, causing the electron density to increase in it [Fang et al., 2008]. This process leads,

say, to the formation of the polar wall of MIT [Galperin et al., 1977; Khalipov et al., 1977] and an additional region of increased electron density inside MIT, called the crest [Besprozvannaya, Benkova, 1988; Zherebtsov et al., 1988]. In [Möller, 1974; Pilkington et al., 1975], BS and satellite data is used to show that the invariant latitude of the crest approximately coincides with the latitudes of the ionospheric projection of the plasmapause and the electron temperature maximum in MIT.

The main reason for the development of geomagnetic storms is the magnetospheric convection field strengthening, which causes the inner boundary of the plasma sheet and the outer boundary of the plasmasphere (plasmapause) to move deep into the magnetosphere [Sergeev, Tsyganenko, 1980; Nishida, 1980]; and their ionospheric projections, toward the equator. Accordingly, MIT, located, according to existing concepts, between the auroral oval and the plasmapause, as well as the electron density irregularities characteristic of MIT, which affect HF radio wave propagation, shift to lower latitudes.

One of the irregularities existing in MIT is a trough in trough — a narrow ionization trough (NIT) related to the polarization jet (PJ), first described in [Galperin et al., 1973; Galperin et al., 1974]. The morphology of

NIT and its relationships with PJ is most fully presented in the monograph [Stepanov et al., 2017]. According to the monograph, in the F-region of the ionosphere, narrow ($\sim 1^\circ$ – 2° wide) ionization troughs are observed 1° – 10° equatorward of DPE outside (in some cases inside) the plasmapause projection. As the disturbance develops, the distance between NIT and DPE decreases. NITs are most pronounced during substorms against the background of enhanced large-scale ionospheric plasma convection. NITs are formed for 15–30 min, exist for several hours, and in cases of substorms propagate rapidly along the longitude, reaching a longitude size of $\sim 100^\circ$ and larger. An increase in geomagnetic activity is accompanied by a decrease in NIT latitude, which together with other factors can lead to a blackout on subauroral paths — absence of radio signal transmission. Note also that PJ induces ionospheric plasma stratification [Sinevich et al., 2023], which can also affect the mode structure of HF signals.

2.1. November 2023

Figure 10 for November 3–17, 2023 illustrates time variations in MOF_{IF} on the Magadan—Irkutsk (a) and Norilsk—Irkutsk (b) paths, invariant latitudes Φ of the

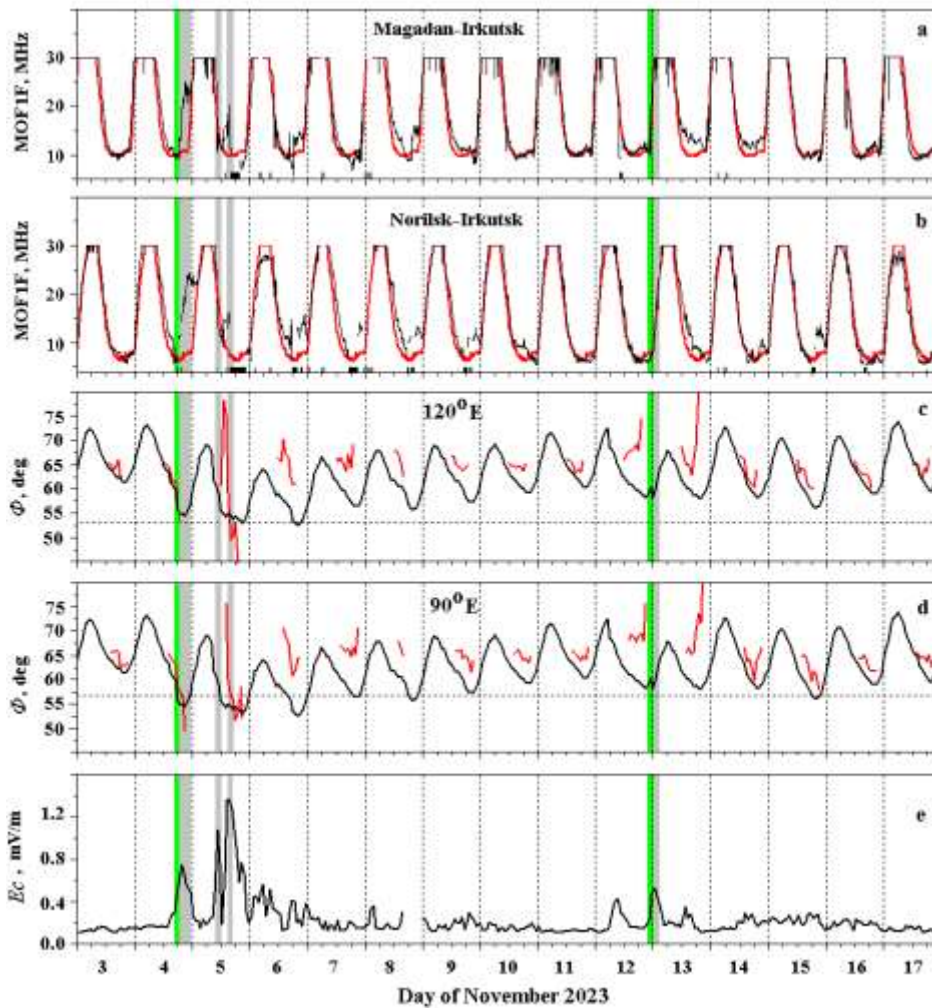


Figure 10. Variations in MOF_{IF} on the Magadan—Irkutsk (a) and Norilsk—Irkutsk (b) paths, invariant geomagnetic latitudes of MIT and DPE at meridians of 120° E (c) and 90° E (d), magnetospheric convection electric field strength (e) for November 3–17, 2023

MIT bottom (black line) and DPE (red line) at the meridians of 120° E (c) and 90° E (d), magnetospheric convection electric field strength (e). Red lines (a, b) are variations in the MOF_{1F} monthly median; gray rectangles along the X-axis are time intervals without measurements; black lines are blackout intervals. Horizontal dotted lines are latitudes of midpoints of the Magadan—Irkutsk ($\Phi=53.3^\circ$) (c) and Norilsk—Irkutsk ($\Phi=56.92^\circ$) (d) paths. Green rectangles represent the initial phases of storms 1 and 2; gray ones, steps of their main phases.

During morning and afternoon hours (LT), medium-scale traveling ionospheric disturbances (TIDs) were constantly recorded on the OS paths considered. The observation period (November, December 2023) of interest featured a high level of solar activity; therefore, MOF of the radio paths in the daytime exceeded the upper edge of the sounding frequency range (30 MHz). Variations in MOF_{1F} (see Figure 10) are limited by the maximum sounding frequency. We do not analyze daytime TIDs. In the evening and after-midnight hours in winter, the probability of occurrence of TIDs is low [Kurkin et al., 2024] and against the background of ionospheric disturbances, driven by magnetic storms, they do not appear in OS ionograms.

Severe geomagnetic storm 1 began on November 4 at 16:45 UT; and its main phase, at ~ 18 UT. From this moment, MOF_{1F} increases (a, b), which is associated with the approach of MIT and DPE to the midpoint of the path (c, d). On the Magadan—Irkutsk path at 18:23 hrs UT along with standard 1F2 and 2F2 signals reflected from the F2 layer, there are additional signals with delays exceeding the delays in the main propagation modes and frequencies higher than MOF_{1F2} in OS ionograms. Figure 11 exhibits OS ionograms illustrating variations and features of the mode structure of the signal on the Magadan—Irkutsk path at 19:35, 20:00, and 21:00 UT. Additional signals are designated as 1F. During these hours, E_c increases (see Figure 10, e). MIT and the diffuse electron precipitation zone shift in latitude to the reflection region at the midpoint of the radio path (see Figure 10, c). Low-energy electron precipitation causes the electron density to increase in the F-region near the polar wall of MIT [Galperin et al., 1977]. An additional region of increased electron density is also formed inside MIT [Zherebtsov et al., 1988]. An increase in the electron density leads to a significant increase in MOF of main propagation modes 1F2 and 2F2 and additional 1F signals. Since the Magadan—Irkutsk path is quasi-

transverse relative to the geomagnetic field direction, the appearance of abnormal 1F signal at 19:35 UT (see Figure 11, a) is due to bistatic scattering by intense small-scale field-aligned irregularities near the polar wall of MIT [Uryadov et al., 2005]. At 20:00 UT, the middle part of the path is located in MIT and in the diffuse precipitation zone. Signals of main mode 1F2 and additional 1F signals become similar in delay (b). As MIT moves away from the midpoint of the path to the north and E_c decreases, the mode structure of signals returns to the standard form (c).

On the Norilsk—Irkutsk path, the effect of ionospheric disturbances on radio wave propagation conditions manifested itself from 17:03 UT. Low-amplitude scattered signals were recorded in OS ionograms and there were individual blackouts due to the low electron density in the F-region and large signal attenuation since part of the propagation path, including the transmission point, was near MIT and diffuse precipitation zone. Changes in the mode structure of recorded signals depend on the position of MIT and DPE relative to the signal reflection regions in the ionosphere. From 19:38 UT, the reflection region of propagation mode 1F2 is located near MIT and diffuse electron precipitation zone (see Figure 10, d). The electron density in the F2 layer increases, thereby causing MOF_{1F2} to increase. Then, DPE and the MIT bottom shift equatorward. Mode 2F2 and additional 1F signal propagating outside the great circle arc appear in OS ionograms. The delay in additional 1F signal exceeds the delay in main mode 1F2, and MOF_{1F} is higher than MOF_{1F2} . Occurrence of additional signals may be attributed to the azimuthal refraction of radio waves in transverse electron density gradients near the polar wall of MIT [Zaalov et al., 2003, 2005]. At subsequent points in time, MIT shifts to the pole and from 22:38 UT OS ionogram takes the standard form. On the Norilsk—Irkutsk path, abnormal diffuse signals of bistatic scattering are not recorded due to the orientation of the path relative to the geomagnetic field direction.

During the second and third steps of the main phase of the severe geomagnetic storm on November 5, ionospheric disturbances on the Magadan—Irkutsk path began to manifest themselves from 10:30 UT. For twenty minutes, abnormal diffuse signals with delays exceeding the signal delays of main mode 1F2 by about 1 ms are recorded. MOF_{1F} and MOF_{1F2} are approximately equal.

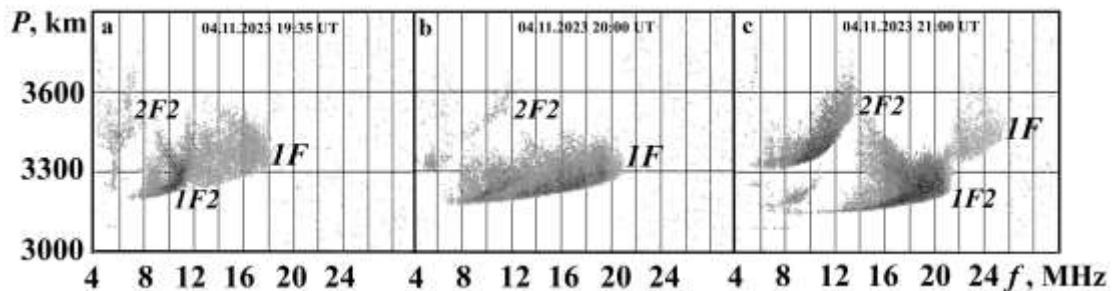


Figure 11. OS ionograms from the Magadan—Irkutsk path for November 4, 2023: a — 19:35 UT; b — 20:00 UT; c — 21:00 UT

Occurrence of such signals is associated with the aspect radio wave scattering by small-scale magnetic field-aligned irregularities near the equatorial boundary of the auroral oval in the diffuse precipitation zone [Uryadov et al., 2004]. In the evening, the equatorial boundary of the auroral oval shifts downward in latitude, and hence the delays in additional 1F signals in ionograms decrease. Closer to 15:00 UT, MIT shifts and covers the ionospheric reflection region for mode 1F2. At the same time, E_c increases to maximum values (see Figure 10, *e*), DPE crosses the middle region of the radio path and shifts downward in latitude (*b*). Signal delays of main mode 1F2 and additional diffuse mode 1F are approximately the same, and $\text{MOF}_{1F} > \text{MOF}_{1F2}$. Next, signal mode 1F2 weakens and disappears. Only the additional 1F signal remains. After DPE shift to latitudes lower than the latitude of the midpoint of the path, and the cessation of electron precipitation into the signal reflection region (see Figure 10, *c*), a complete blackout occurs at 16:20–19:55 UT, which is associated with a decrease in the electron density. From 20:00 UT, the mode structure of the signals recorded in OS ionograms is reconstructed to the form standard for undisturbed conditions.

On the Norilsk—Irkutsk path during the main phase of storm 1, most of the path was in MIT and in the diffuse precipitation zone starting at 10:33 UT on November 5, 2023; therefore, ionograms with weak scattered signals and ionograms with blackouts were recorded (Figure 10, *b*).

During weak magnetic storm 2 (November 12–14, 2023) on both sounding paths, MOF_{1F} variations relative to the diurnal median of measurements are associated with the position of MIT and DPE with respect to the reflecting regions of the ionosphere and variations in the convection field strength. On the Magadan—Irkutsk path, MIT was located far from the propagation path; therefore, scattered 1F signals were not detected in ionograms. Main variations in MOF_{1F} at night were governed by medium-scale TIDs. On the Norilsk—Irkutsk path, the increases in MOF_{1F} in the afternoon of November 14 and 15 are associated with the approach of MIT and DPE to the midpoint of the path, which led to the formation of an additional 1F signal reflected from the polar wall of the trough.

Figure 12 illustrates time variations in MOF_{1F} on the paths Magadan—Irkutsk (*a*) and Norilsk—Irkutsk (*b*), latitudes Φ for the MIT bottom and DPE at the meridians of 120° E (*c*) and 90° E (*d*), and E_c (*e*) for November 21–27, 2023. For moderate magnetic storm 3 (November 21–23, 2023), MOF_{1F} variations in the evening and at night along the Magadan—Irkutsk path are due to recording of additional 1F signals with delays exceeding the delays in main propagation mode 1F2 and frequencies higher than MOF_{1F2} .

During the main phase of moderate magnetic storm 4 (November 25, 2023), an increase in E_c (*e*) and electron precipitation led to the formation of regions of aspect scattering by field-aligned irregularities on the polar wall of MIT in the evening hours (LT), which generated additional signals in OS ionograms on the Magadan—Irkutsk path and hence caused an increase in MOF_{1F} .

Weak scattered signals and long blackout intervals (*b*) were detected on the Norilsk—Irkutsk path during magnetic storms 3, 4.

2.2. December 2023

Examine disturbances of the ionospheric radio channel during magnetic storms in December 2023. Figure 13 exhibits time variations in MOF_{1F} of one hop mode on the Magadan—Irkutsk (*a*) and Norilsk—Irkutsk (*b*) paths, latitudes Φ of the MIT bottom (black line) and DPE (red line) at the meridians of 120° E (*c*) and 90° E (*d*), and E_c (*e*) for November 30–December 7, 2023. A distinctive feature of severe magnetic storm 5 (December 1–7, 2023) is abnormally high values of the convection electric field strength and a marked equatorward shift in MIT. According to the dynamics of changes in the latitude of the MIT bottom (*c*), on December 1, 2023 the middle part of the Magadan—Irkutsk path was in MIT for more than 12 hrs (12–24 UT). The middle part of the Norilsk—Irkutsk path was in MIT for ~15 hrs (*d*). There were large variations in MOF of propagation modes relative to their median values (*a*, *b*).

Figure 14 presents OS ionograms obtained from the Magadan—Irkutsk path for 12:00 UT, 16:45 UT, and 22:00 UT on December 1, which can be used to track changes and features of the signal mode structure, which are associated with ionospheric disturbances during

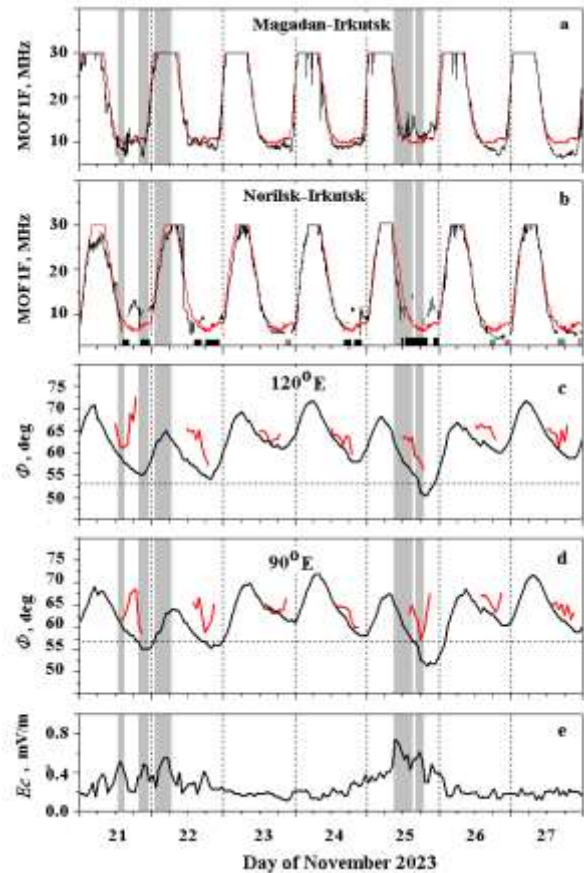


Figure 12. Variations on MOF_{1F} on the Magadan—Irkutsk (*a*) and Norilsk—Irkutsk (*b*) paths, invariant geomagnetic latitudes of MIT and DPE at the meridians of 120° E (*c*) and 90° E (*d*), and E_c (*e*) for November 21–27, 2023

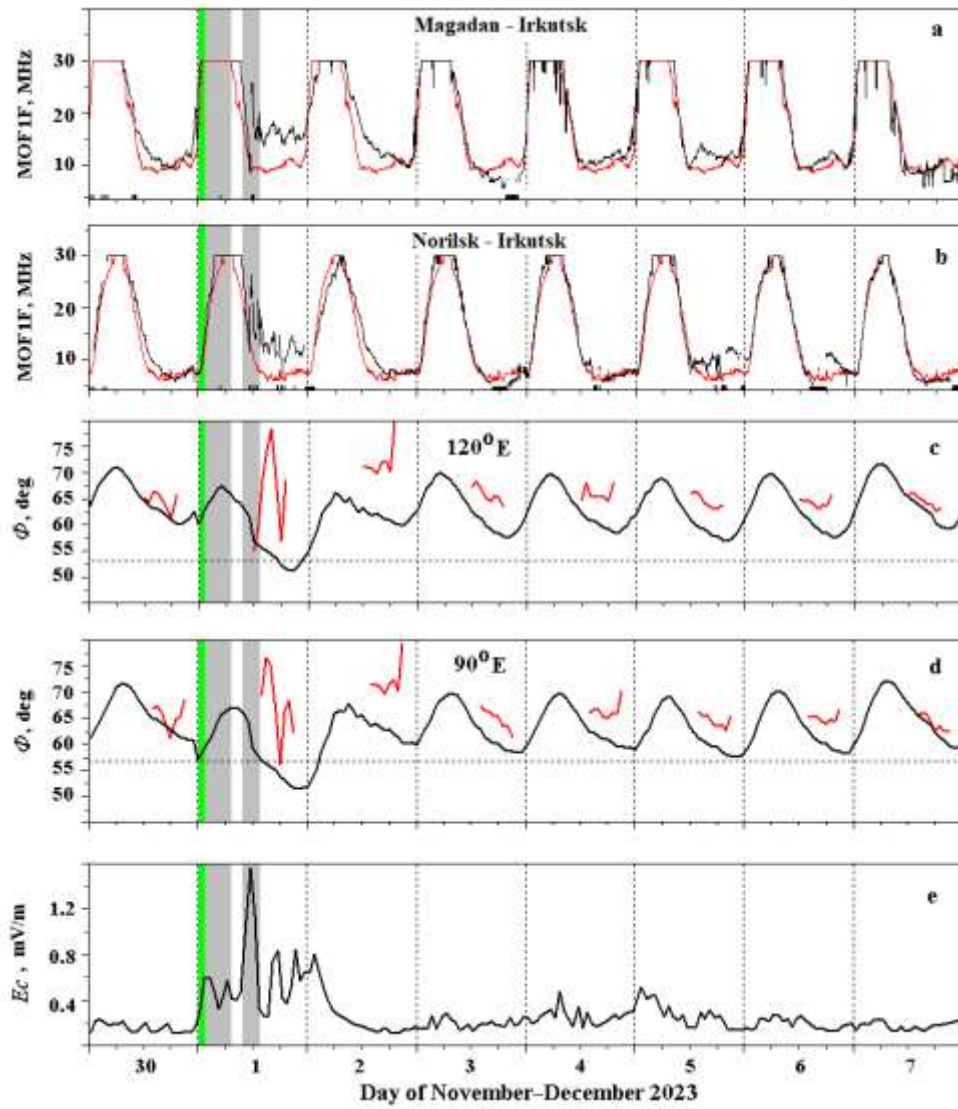


Figure 13. Time variations in MOF_{IF} on the Magadan—Irkutsk (a) and Norilsk—Irkutsk (b) paths, invariant geomagnetic latitudes of MIT, and DP zone edge at meridians of 120° (c) and 90° (d), magnetospheric convection electric field strength (e) for November 30 – December 7, 2023

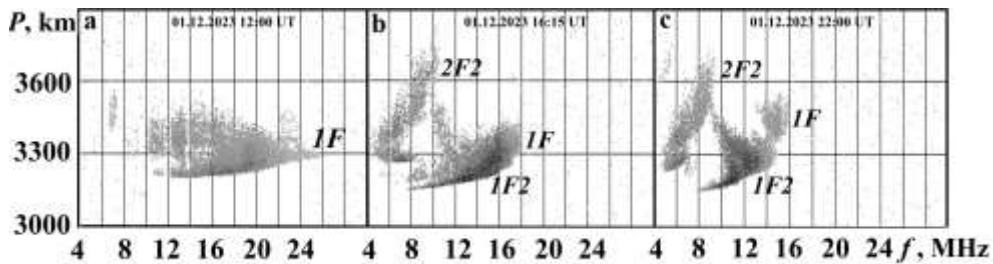


Figure 14. OS ionograms from the Magadan—Irkutsk path on December 1, 2023 at 12:00 (a), 16:15 (b), 22:00 UT (c)

this magnetic storm. As for magnetic storm 4, enhancement of the magnetospheric convection electric field (see Figure 13, e) and electron precipitation brought about the formation of regions of aspect scattering by field-aligned irregularities at the equatorial boundary of the auroral oval during the evening hours (LT). Starting at 10:50 UT on December 1, 2023, additional signals with delays and MOF exceeding the delays and MOF of the main propagation modes were recorded. In half an hour, MIT

covered the middle part of the path. At the same time, DPE shifted in latitude to the midpoint of the path and the region of the ionosphere reflecting propagation mode 1F2 appeared in the diffuse precipitation zone. Indeed, according to the analysis of experimental ionograms, the middle part of the Magadan—Irkutsk path on December 1, 2023 was in the MIT zone for about 10 hrs from 11:20 to 21:20 UT. The shift of MIT and DPE to the middle part of the path led in total to an increase in

the electron density in the reflecting F layer, followed by an increase in MOF_{1F} (Figure 14, *a, b*). As E_c changes, MOF_{1F} changes too. It can be seen (Figure 13) that at 12–24 UT on December 1 there were three intervals of intensification of MOF_{1F} fluctuations on the Magadan—Irkutsk path, which were close in duration to the E_c oscillation periods of ~ 4 hrs. Further, as MIT shifts to the north, additional 1F signals related to radio wave scattering by the polar wall of the trough are recorded in OS ionograms (see Figure 14, *c*). From 23:35 UT on December 1, the mode structure of the signals in the ionograms recovers to the standard form determined by solar radiation during the morning hours (LT).

On the Norilsk—Irkutsk path, the mode structure of the recorded HF signals during the main phase of storm 5 also depends on the position of MIT and DPE relative to the propagation path. Starting at 10:48 UT on December 1, additional signals appear in OS ionograms due to the azimuthal refraction of radio waves in transverse electron density gradients near the polar wall of MIT. At 11:38 UT, the diffuse precipitation zone is located in MIT and the convection electric field strength increases sharply (see Figure 13, *e*). Main mode 1F2 and additional mode 1F1 become similar in delay, MOF_{1F} increases due to the additional electron density in the F-region of the ionosphere. Further, from 12:23 UT, most of the path is located in the

electron precipitation zone, as evidenced by the appearance of a reflective E_s layer in OS ionograms from 15:58 to 17:08 UT. Signals are reflected due to precipitation of electrons in the E- and F-regions. The recorded signals reflected from the F-region are diffuse. Variations in MOF_{1F} for the evening and night periods (LT) (see Figure 13, *b*) result from variations in E_c (*e*).

During magnetically disturbed days on December 2–6, 2023, ionograms with weak scattered signals or blackout periods were recorded in the evening and night hours along both OS paths.

A feature of the December 13–18 magnetic disturbances was a relatively high level of $E_c > 0.4$ mV/m (Figure 15, *e*). Influx of electrons into the upper ionosphere in combination with the motion of MIT and DPE toward the midpoints of the radio paths causes variations in MOF of propagation modes during evening and night hours (LT). Low-amplitude signals were recorded in OS ionograms. There was often a blackout during the night hours. The blackout intervals are marked with black rectangles (*a, b*).

The highest variations in MOF_{1F} on the sounding paths were observed on December 17 and 18. On the Magadan—Irkutsk path, an increase in MOF_{1F} from 17:00 UT on December 17 is associated with a shift of MIT and DPE to the latitudes of the reflecting regions

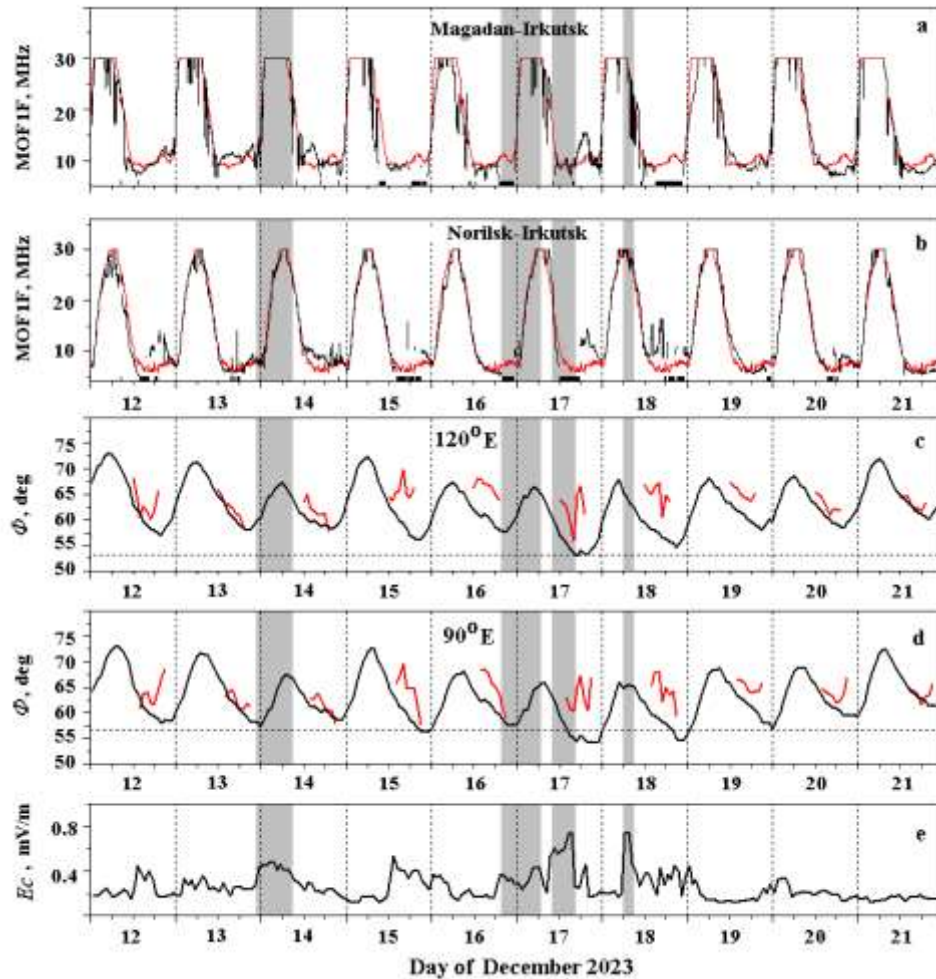


Figure 15. Variations in MOF_{1F} on the Magadan—Irkutsk (*a*) and Norilsk—Irkutsk (*b*) paths; invariant geomagnetic latitudes of MIT, and DP zone edge at the meridians of 120° E (*c*) and 90° E (*d*); E_c (*e*) for December 12–21, 2023

of the ionosphere for signals of mode 1F2. Together with the increase in the convection electric field strength E_c (e), this causes the electron density to increase in the F-region. On the Norilsk—Irkutsk path, a nighttime increase in MOF_{1F} is associated with the passage of radio waves through the diffuse low-energy electron precipitation zone. During evening and night hours of December 18 there was a blackout on both paths (a , b).

CONCLUSION

We have examined features of the manifestation of heliogeospheric interaction in OS data obtained from the subauroral HF radio paths Magadan—Irkutsk and Norilsk—Irkutsk during geomagnetic storms in November–December 2023. Analysis of the results of processing of ionospheric sounding data by a continuous chirp signal together with data from modeling of the spatial position of the MIT bottom, the equatorial edge of diffuse electron precipitation, and magnetospheric convection electric field strength has shown the following.

1. During severe and moderate magnetic storms in November–December 2023, ionospheric disturbances generate strong variations in MOF of HF radio wave propagation on the subauroral paths Magadan—Irkutsk and Norilsk—Irkutsk during evening and night hours (LT). The MOF variations depend on the position of MIT and DPE relative to the midpoint of the radio path during strengthening of the magnetospheric convection electric field.

2. During evening and night hours, additional signals with delays and MOF exceeding the corresponding parameters of standard one hop radio wave propagation modes under undisturbed conditions are recorded in OS ionograms. The appearance of additional signals on the Magadan—Irkutsk path may be due to the refraction of radio waves near MIT, as well as scattering by small-scale field-aligned irregularities, near the equatorial boundary of the auroral oval or near MIT.

3. Ionospheric disturbances linked to diffuse electron precipitation and variations in the magnetospheric convection electric field strength lead to the absence of radio waves passing along subpolar paths during evening and night hours (LT).

The work was financially supported by the Ministry of Science and Higher Education of the Russian Federation (Subsidy No. 075-GZ/Ts3569/278). The experimental data was obtained using the equipment of Shared Equipment Center «Angara» [<http://ckp-rf.ru/ckp/3056/>].

REFERENCES

Akasofu S.I. Energy coupling between the solar wind and the magnetosphere. *Space Sci. Rev.* 1981, vol. 28, pp. 121–190. DOI: [10.1007/BF00218810](https://doi.org/10.1007/BF00218810).

Basler R.P., Price G.H., Tsunoda R.T., Wong T.L. Ionospheric distortion of HF signals. *Radio Sci.* 1988, vol. 23, no 4, pp. 569–579. DOI: [10.1029/RS023i004p00569](https://doi.org/10.1029/RS023i004p00569).

Bergin A., Chapman S.C., Gjerloev J.W. AE, DST, and their SuperMAG counterparts: The effect of improved spatial resolution in geomagnetic indices. *J. Geophys. Res.* 2020, vol. 125, e2020JA027828. DOI: [10.1029/2020JA027828](https://doi.org/10.1029/2020JA027828).

Besprozvannaya A.S., Ben'kova N.P. Large-scale structural features of the F2 layer at high latitudes *Proc. International Symposium "Physical Processes in the Trough Region during Disturbances"*. Garzau, Germany (31.03-04.04.1987). Berlin, 1988, pp. 25–39. (In Russian).

Blagoveshchenskii D.V. Effect of magnetic storms (substorms) on HF propagation: A review. *Geomagnetism and Aeronomy.* 2013, vol. 53, no. 4, pp. 409–423. DOI: [10.1134/S0016793213040038](https://doi.org/10.1134/S0016793213040038).

Blagoveshchenskii D.V. Anomalous phenomena on HF radio paths during geomagnetic disturbances. *Geomagnetism and Aeronomy.* 2016, vol. 56, no. 4, pp. 448–456. DOI: [10.1134/S0016793216040022](https://doi.org/10.1134/S0016793216040022).

Blagoveshchensky D.V., Borisova T.D. Substorm effects of ionosphere and propagation. *Radio Sci.* 2000, vol. 35, no. 5, pp. 1165–1171. DOI: [10.1029/1998RS001776](https://doi.org/10.1029/1998RS001776).

Blagoveshchensky D.V., Zherebtsov G.A. *High-Latitude Geophysical Phenomena and Prediction of Short-Wave Radio Channels*. Moscow, Nauka Publ., 1987, 272 p. (In Russian).

Blagoveshchensky D.V., Kalishin A.S., Sergeeva M.A. Space weather effects on radio propagation: study of the CEDAR, GEM and ISTP storm events. *Ann. Geophys.* 2008, vol. 26, iss. 6, pp. 1479–1490. DOI: [10.5194/angeo-26-1479-2008](https://doi.org/10.5194/angeo-26-1479-2008).

Burke W.J., Huang C.Y., Marcos F.A., Wise J.O. Interplanetary control of thermospheric densities during large magnetic storms. *J. Atmos. Solar-Terr. Phys.* 2007, vol. 69, iss. 3, pp. 279–287. DOI: [10.1016/j.jastp.2006.05.027](https://doi.org/10.1016/j.jastp.2006.05.027).

Burton R.K., McPherron R.L., Russell C.T. An empirical relationship between interplanetary conditions and *Dst*. *J. Geophys. Res.* 1975, vol. 80, no. 31, pp. 4204–4214. DOI: [10.1029/JA080i031p04204](https://doi.org/10.1029/JA080i031p04204).

Davis K. *Radio Waves in the Ionosphere*. Moscow, Mir Publ., 1973. 502 p. (In Russian).

Davies E.E., Forsyth R.J., Good S.W., Kilpua E.K.J. On the radial and longitudinal variation of a magnetic cloud: ACE, Wind, ARTEMIS and Juno observations. *Solar Phys.* 2020, vol. 295, article number 157. DOI: [10.1007/s11207-020-01714-z](https://doi.org/10.1007/s11207-020-01714-z).

Deminov M.G., Shubin V.N. Empirical model of the location of the main ionospheric trough. *Geomagnetism and Aeronomy.* 2018, vol. 58, no. 3, pp. 348–355. DOI: [10.1134/S0016793218030064](https://doi.org/10.1134/S0016793218030064).

Dremuhina L.A., Lodkina I.G., Ermolaev Ju.I. Correlation between solar wind parameters of different types and geomagnetic activity indices in 1995–2016. *Proc. XLI Annual Seminar "Physics of Auroral Phenomena"*. Apatity (12–16 March 2018), pp. 34–37. DOI: [10.25702/KSC.2588-0039.2018.41.34-37](https://doi.org/10.25702/KSC.2588-0039.2018.41.34-37). (In Russian).

Fang X., Randall C.E., Lummerzheim D., Solomon S.C., Mills M.J., Marsh D.R., et al. Electron impact ionization: A new parameterization for 100 eV to 1 MeV electrons. *J. Geophys. Res.: Space Phys.* 2008, vol. 113, A09311. DOI: [10.1029/2008JA013384](https://doi.org/10.1029/2008JA013384).

Galperin Yu.I., Ponomarev Ju.N., Zosimova A.G. Direct measurements of drift rate of ions in upper atmosphere during a magnetic storm. *Cosmic Res.* 1973, vol. 11, no. 2, p. 240.

Galperin Yu.I., Ponomarev V.N., Zosimova A.G. Plasma convection in the polar ionosphere. *Ann. Geophys.* 1974, vol. 30, no. 1, pp. 1–7.

Galperin Iu.I., Crasnier J., Sauvaud J.-A., Lisakov Iu.V., Nikolaenko L.M., Sinityn V.M., Khalipov V.L. The diffuse auroral zone. I - A model for the equatorial boundary of the diffuse surge zone of auroral electrons in the evening and midnight sectors. *Cosmic Res.* 1977, vol. 15, no. 3, pp. 362–374.

Gonzalez W.D., Joselyn J.A., Kamide Y., Kroehl H.W., Rostoker G., Tsurutani B.T. et al. What is a geomagnetic storm? *J. Geophys. Res.* 1994, vol. 99, iss. A4, pp. 5771–5792. DOI: [10.1029/93JA02867](https://doi.org/10.1029/93JA02867).

- Grozov V.P., Ilyin N.V., Kotovich G.V., Ponomarchuk S.N. Software system for automatic interpretation of ionosphere sounding data. *Pattern Recognition and Image Analysis*. 2012, vol. 22, no. 3, pp. 458–463. DOI: [10.1134/S1054661812030042](https://doi.org/10.1134/S1054661812030042).
- Hunsucker R.D., Bates H.F. Survey of polar and auroral region effects on HF propagation. *Radio Sci.* 1969, vol. 4, no. 4, pp. 347–365. DOI: [10.1029/RS004i004p00347](https://doi.org/10.1029/RS004i004p00347).
- Hunsucker R.D., Hargreaves J.K. *The High-Latitude Ionosphere and Its Effects on Radio Propagation*. Cambridge University Press, 2003, 617 p. DOI: [10.1017/CBO9780511535758](https://doi.org/10.1017/CBO9780511535758).
- Joselyn J.A., Tsurutani B.T. Geomagnetic sudden impulses and storm sudden commencement. A note on terminology. *Eos, Transactions American Geophysical Union*. 1990, vol. 71, iss. 47, pp. 1808–1811. DOI: [10.1029/90EO00350](https://doi.org/10.1029/90EO00350).
- Kamide Y., Winningham J.D. A statistical study of the “instantaneous” nightside auroral oval: The equatorward boundary of electron precipitation as observed by the Isis 1 and 2 satellites. *J. Geophys. Res.* 1977, vol. 82, iss. 35, pp. 5573–5588. DOI: [10.1029/JA082i035p05573](https://doi.org/10.1029/JA082i035p05573).
- Kamide Y., Yokoyama N., Gonzalez W., Tsurutani B.T., Daglis I.A., Brekke A., Masuda S. Two-step development of geomagnetic storms. *J. Geophys. Res.* 1998, vol. 103, iss. A4, pp. 6917–6921. DOI: [10.1029/97JA03337](https://doi.org/10.1029/97JA03337).
- Khalipov V.L., Galperin Iu.I., Lisakov Iu.V., Krane Zh., Nikolaenko L.M., Sinityn V.M., Sovo Zh.-A. Diffuse auroral zone. II - Formation and dynamics of the polar rim of the sub-auroral ionospheric trough in the nighttime sector. *Cosmic Res.* 1977, vol. 15, no. 5, pp. 708–724. (In Russian).
- Kilpua E., Koskinen H.E.J., Pulkkinen T.I. Coronal mass ejections and their sheath regions in interplanetary space. *Living Rev. Solar Phys.* 2017, vol. 14, article number 5. DOI: [10.1007/s41116-017-0009-6](https://doi.org/10.1007/s41116-017-0009-6).
- Kurkin V.I., Ponomarchuk S.N., Smirnov V.F. On influence of the main ionospheric trough on SW-signal characteristics on routes of tilt sounding. *Solnechno-zemnaja fizika [Solar-Terrestrial Phys.]*. 2004, iss. 5, pp. 124–127. (In Russian).
- Kurkin V.I., Matyushonok S.M., Pirog O.M., Poddelsky I.N., Ponomarchuk S.N., Rozanov S.V., Smirnov V.F. The dynamics of the auroral oval and ionospheric trough boundaries according to data from the DMSP satellites and ground-based ionosonde network. *Adv. Space Res.* 2006, vol. 38, no. 8, pp. 1772–1777. DOI: [10.1016/j.asr.2006.03.023](https://doi.org/10.1016/j.asr.2006.03.023).
- Kurkin V.I., Medvedeva I.V., Podlesnyi A.V. Effect of sudden stratosphere warming on characteristics of medium-scale traveling ionospheric disturbances in the Asian region of Russia. *Adv. Space Res.* 2024, vol. 73, no. 7, pp. 3613–3623. DOI: [10.1016/j.asr.2023.09.020](https://doi.org/10.1016/j.asr.2023.09.020).
- Loewe C.A., Prolss G.W. Classification and mean behavior of magnetic storm. *J. Geophys. Res.* 1997, vol. 102, no. A7, pp. 14209–14213. DOI: [10.1029/96JA04020](https://doi.org/10.1029/96JA04020).
- Möller H.G. Backscatter results from Lindau-II. The movement of curtains of intense irregularities in the polar F-layer. *J. Atmos. Terr. Phys.* 1974, vol. 36, no. 9, pp. 1487–1501. DOI: [10.1016/0021-9169\(74\)90227-X](https://doi.org/10.1016/0021-9169(74)90227-X).
- Nishida A. *Geomagnetic Diagnosis of the Magnetosphere*. Springer Nature, 1978, 256 p.
- Pilkington G.R., Münch J.W., Braun H.J., Möller H.G. Comparison of ground HF backscatter and simultaneous particle and plasma pause measurements from a polar orbiting satellite. *J. Atmos. Terr. Phys.* 1975, vol. 37, no. 2, pp. 337–347. DOI: [10.1016/0021-9169\(75\)90115-4](https://doi.org/10.1016/0021-9169(75)90115-4).
- Podlesnyi A.V., Bryn'ko I.G., Kurkin V.I., Berezovsky V.A., Kiselev A.M., Petukhov E.V. Multifunctional chirp ionosonde for ionosphere monitoring. *Geliogeofizicheskie issledovaniya [Heliogeophysical Res.]*. 2013, no. 4, pp. 24–31. (In Russian).
- Polekh N.M., Zolotukhina N.A., Romanova E.B., S. N. Ponomarchuk, Kurkin V.I., Podlesnyi A.V. Ionospheric effects of magnetospheric and thermospheric disturbances on March 17–19, 2015. *Geomagnetism and Aeronomy*. 2016, vol. 56, no. 5, pp. 557–571. DOI: [10.1134/S0016793216040174](https://doi.org/10.1134/S0016793216040174).
- Ponomarchuk S.N., Grozov V.P. Automatic interpretation of oblique sounding ionograms based on hybrid algorithms. *Solar-Terr. Phys.* 2024, vol. 10, iss. 2, pp. 102–110. DOI: [10.12737/stp-102202410](https://doi.org/10.12737/stp-102202410).
- Ponomarchuk S.N., Kurkin V.I., Ilyin N.V., Penzin M.S. HF radio path modeling by waveguide approach. *Solar-Terr. Phys.* 2024, vol. 10, iss. 2, pp. 93–101. DOI: [10.12737/stp-102202409](https://doi.org/10.12737/stp-102202409).
- Richardson I.G., Zhang J. Multiple-step geomagnetic storms and their interplanetary drivers. *Geophys. Res. Lett.* 2008, vol. 35, article number L06S07. DOI: [10.1029/2007GL032025](https://doi.org/10.1029/2007GL032025).
- Rogers N.C., Warrington E.M., Jones T.B. Large HF bearing errors for propagation paths tangential to auroral oval. *IEEE Proceedings-Microwaves, Antennas and Propagation*. 1997, vol. 144, no. 2, pp. 91–96. DOI: [10.1049/ip-map:19970663](https://doi.org/10.1049/ip-map:19970663).
- Rogers N.C., Warrington E.M., Jones T.B. Oblique ionogram features associated with off-great circle HF propagation at high and sub-auroral latitudes. *Proc. IEEE, Microwaves, Antennas and Propagation*. 2003, vol. 150, no. 4, pp. 295–300. DOI: [10.1049/ip-map:20030552](https://doi.org/10.1049/ip-map:20030552).
- Sergeev V.A., Tsyganenko N.A. *Magnitosfera Zemli [Earth's Magnetosphere]*. Moscow, Nauka Publ., 1980, 174 p. (In Russian).
- Sinevich A.A., Chernyshov A.A., Chugunin D.V., Moglevsky M.M., Miloch W.J. The internal structure of a polarization jet/SAID: A stratified polarization jet/SAID. *Geomagnetism and Aeronomy*. 2023, vol. 63, no. 6, pp. 747–756. DOI: [10.1134/S0016793223600583](https://doi.org/10.1134/S0016793223600583).
- Stepanov A.E., Halipov V.L., Golikov I.A., Bondar E.D. *Polarization Jet: Narrow and Fast Drifts of Subauroral Ionospheric Plasma*. Yakutsk, SVFU Publ., 2017, 176 p. (In Russian).
- Uryadov V.P., Kurkin V.I., Vertogradov G.G., Vertogradov V.G., Ponyatov A.A., Ponomarchuk S.N. Features of propagation of HF signals on mid-latitude paths under conditions of geomagnetic disturbances. *Radiophysics and Quantum Electronics*. 2004, vol. 47, no. 12, pp. 933–946.
- Uryadov V.P., Ponyatov A.A., Vertogradov G.G., Vertogradov V.G., Kurkin V.I., Ponomarchuk S.N. Dynamics of the auroral oval during geomagnetic disturbances observed by oblique sounding of the ionosphere in the Eurasian longitudinal sector. *International J. Geomagnetism and Aeronomy*. 2005, vol. 6, G11002. DOI: [10.1029/2004GI000078](https://doi.org/10.1029/2004GI000078).
- Warrington E.M., Rogers N.C., Stocker A.J., Siddle D.R., Al-Behadili H.A.H., Honary F., et al. Developments in HF propagation predictions to support communications with aircraft on transpolar routes. *2017 Progress in Electromagnetics Research Symposium-Spring (PIERS)*. IEEE, 2017, pp. 1953–1959. DOI: [10.1109/PIERS.2017.8262070](https://doi.org/10.1109/PIERS.2017.8262070).
- Zaalov N.Y., Warrington E.M., Stocker A.J. The simulation of off-great circle HF propagation effects due to the presence of patches and arcs of enhanced electron density within the polar cap ionosphere. *Radio Sci.* 2003, vol. 38, no. 3, p. 18. DOI: [10.1029/2002RS002798](https://doi.org/10.1029/2002RS002798).
- Zaalov N.Y., Warrington E.M., Stocker A.J. A ray-tracing model to account for off-great circle HF propagation over northerly paths. *Radio Sci.* 2005, vol. 40, RS4006, pp. 1–14. DOI: [10.1029/2004RS003183](https://doi.org/10.1029/2004RS003183).
- Zhao H., Zong Q.G., Wei Y., Wang Y. Influence of solar wind dynamic pressure on geomagnetic *Dst* index during various magnetic storms. *Science China Technological Sciences*. 2011, vol. 54, pp. 1445–1454. DOI: [10.1007/s11431-011-4319-y](https://doi.org/10.1007/s11431-011-4319-y).
- Zherebtsov G.A., Mizun Ju.G., Mingalev V.S. *Physical Processes in the Polar Ionosphere*. Moscow, Nauka Publ., 1988, 232 p. (In Russian).
- URL: <https://kp.gfz-potsdam.de/en/data> (accessed February 15, 2024).

URL: https://wdc.kugi.kyoto-u.ac.jp/dst_realtime/index.html (accessed February 14, 2024).

URL: https://cdaweb.gsfc.nasa.gov/cdaweb/istp_public/ (accessed February 15, 2024).

URL: <http://supermag.jhuapl.edu/indices/> (accessed April 18, 2024).

URL: <ftp://ftp.swpc.noaa.gov/pub/warehouse/> (accessed January 15, 2024).

URL: http://www.solen.info/solar/old_reports/ (accessed January 14 января 2024).

URL: http://www.solen.info/solar/coronal_holes.html (accessed April 8 2024).

URL: https://cdaw.gsfc.nasa.gov/CME_list/ (accessed April 8, 2024).

URL: <http://ckp-rf.ru/ckp/3056/> (accessed January 14, 2024).

Original Russian version: Ponomarchuk S.N., Zolotukhina N.A., published in *Solnechno-zemnaya fizika*. 2024. Vol. 10. No. 4. P. 91–105. DOI: [10.12737/szf-104202410](https://doi.org/10.12737/szf-104202410). © 2024 INFRA-M Academic Publishing House (Nauchno-Izdatelskii Tsentr INFRA-M)

How to cite this article

Ponomarchuk S.N., Zolotukhina N.A. Disturbances of ionospheric radio channel during magnetic storms in November–December 2023. *Solar-Terrestrial Physics*. 2024. Vol. 10. Iss. 4. P. 84–98. DOI: [10.12737/stp-104202410](https://doi.org/10.12737/stp-104202410).